chemistry

MDPI

Article

Methylene Blue Removal by Copper Oxide Nanoparticles Obtained from Green Synthesis of *Melia azedarach*: Kinetic and Isotherm Studies

Wafa K. Essa

College of Science, University of Duhok, Duhok 42001, Iraq; wafa.k.essa@uod.ac

Abstract: In this study, *Melia azedarach* fruit extract was used as a reducing agent and copper chloride dihydrate ($CuCl_2 \cdot 2H_2O$) was used as a precursor in the synthesis of copper oxide nanoparticles (CuO NPs). The UV–visible spectrum showed a characteristic absorption peak of CuO NPs at 350 nm. The surface properties of the adsorbent were analyzed through various techniques, indicating the successful formation of CuO NPs. The impacts of several factors, including initial pH (4 to 8), a dose of CuO NPs adsorbent (0.01–0.05 g), dye initial concentration (10–50 $mg \cdot L^{-1}$), and contact times ranging from 5 to 120 min, were examined in batch adsorption studies. Based on the experimental results, the Langmuir isotherm is well-fitted, indicating MB dye monolayer capping on the CuO NPs surface with 26.738 $mg \cdot g^{-1}$ as a maximum adsorption capacity Q_m value. For the pseudo-second-order kinetic model, the experimental and calculated adsorption capacity values (q_e) exhibited good agreement.

Keywords: green synthesis; copper oxide nanoparticles; methylene blue; batch adsorption; water treatment

Citation: Essa, W.K. Methylene Blue Removal by Copper Oxide Nanoparticles Obtained from Green Synthesis of *Melia azedarach*: Kinetic and Isotherm Studies. *Chemistry* **2024**, *6*, 249–263. https://doi.org/10.3390/chemistry6010012

Academic Editors: Andreas Taubert and Emmanuel Unuabonah

Received: 30 December 2023
Revised: 18 January 2024
Accepted: 8 February 2024
Published: 19 February 2024

1. Introduction

A cationic dye belonging to the thiazine dye family, methylene blue (MB), finds widespread applications in the textile, paper, and leather industries, as well as biological dyes [1]. However, the discharge of MB and its derivatives into the environment has led to significant pollution issues. Consumption of MB dye by humans or animals may result in eye burns, fast breathing, vomiting, and nausea. Therefore, it is crucial to remove it from wastewater [2]. Several effective wastewater treatment techniques for dye removal, such as flocculation or coagulation [3], adsorption membranes [4], biological treatment [5], electrochemical processes [6], and photodegradation [7], have been effectively adopted.

Recently, there has been a lot of interest in multifunctional materials due to the advancement of civilization and the growing need for smart materials. These materials were used to eliminate hazardous substances in the natural environment [8,9]. Nano-adsorbents are a highly effective technology for eliminating organic dyes from water and wastewater. Their smaller size and increased adsorptive surface area make them particularly effective in this regard [10]. Nanofibers, graphene, metal oxides, and carbon nanotubes are all examples of nano-adsorbents that can be used to improve the treatment of water and wastewater [11].

Copper oxide nanoparticles (CuO NPs) are a type of metal oxide nanoparticles that have potential applications in both science and industry [12–15]. Various techniques for synthesizing CuO NPs include sonochemical methods [16], chemical precipitation [17], laser ablation in liquid [18], hydrothermal [19], sol-gel [20], and more. The chemical synthesis methods mentioned above are highly effective but have several limitations, such as high costs, utilization of hazardous chemicals and solvents, production of toxic waste, and high energy requirements. As a result, biosynthesis and other economical, environmentally friendly, biocompatible, and reliable approaches for producing nanoparticles have been developed.

Scientists often use plant extracts as a reducing agent to create metal oxide nanoparticles [21–25]. These extracts are highly efficient, accessible, safe, and contain bioactive components [26]. Plant extracts are rich sources of natural phytoconstituents that possess different reductive capacities. During green synthesis, they can serve the dual purpose of both reducing and stabilizing agents. CuO NPs have been synthesized using various plant extracts derived from seeds, fruits, barks, leaves, stems, flowers, roots, and peels, such as *Catha edulis* [27], *Phoenix dactylifera* [28], *Lantana camara* [29], *Bergenia ciliata* [30], *Eucalyptus globulus* [31], *Bougainvillea* [32], and *Papaya* peel [26].

Melia azedarach, also known as chinaberry, is a tree species belonging to the Meliaceae family. It is native to Southeast Asia and Northern Australia and has been introduced to the Kurdistan region of Iraq. This tree is excellent for urban greening as it can absorb harmful and toxic gases and is also resistant to dust and smoke [33]. Extracts from the leaves, fruits, and seeds of *Melia azedarach* have shown medicinal and pesticide properties against various pathogens and pests, respectively [34–36].

In the current research, for the first time, CuO NPs were synthesized using an aqueous extract from the *Melia azedarach* fruit. The effectiveness of the production process was demonstrated by investigating the adsorbent surface using various techniques. By calculating and analyzing equilibrium, kinetic, and isotherm parameters, the adsorption process was thoroughly explained. The results indicate that the environmentally friendly manufacture of CuO nanoparticles as an adsorbent shows great promise for successfully removing MB dye from aqueous solutions. This study is valuable for the protection and management of drinking water. Scheme 1 provides a schematic representation of the current work.

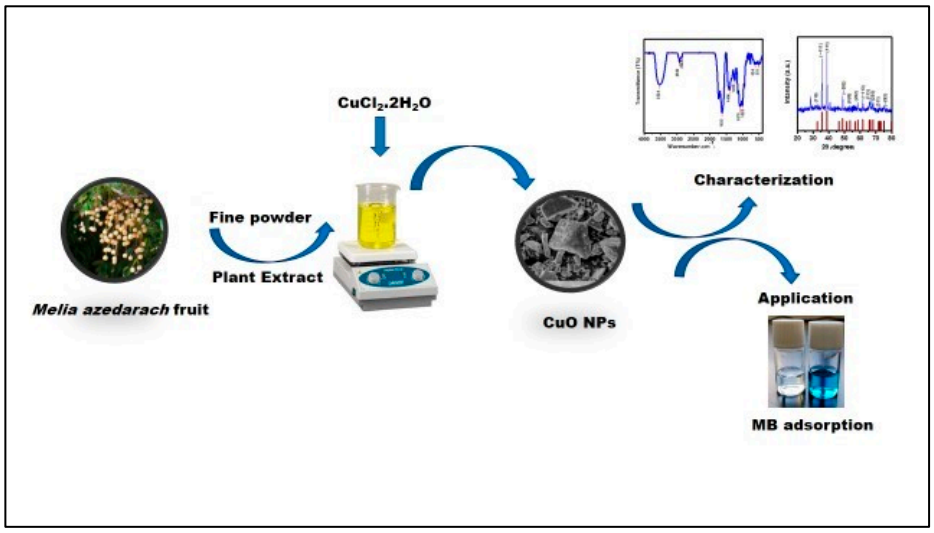

Scheme 1. CuO NPs adsorbent synthesis for MB dye removal.

2. Experimental methodology

2.1. Chemicals and Materials

Dried *Melia azedarach* fruits were collected from the University of Duhok College of Science gardens in Kurdistan, Region of Iraq. Copper chloride dihydrate ($CuCl_2 \cdot 2H_2O$) was purchased from UNI-CHEM (Maharashtra, India). Methylene blue MB dye (chemical formula $C_{16}H_{18}N_3SCl \cdot 3H_2O$, λmax = 660 nm and molecular weight = 319.85 $g \cdot mol^{-1}$), hydrochloric acid (HCl), and sodium hydroxide (NaOH), of 99% purity, were purchased from the German Sigma-Aldrich Company (Steinheim, Germany). The extract from the *Melia azedarach* fruits and the metal salt solution were prepared using distilled water (D.W).

2.2. Preparation of Melia azedarach Fruit Extract

Dried fruit of *Melia azedarach* were collected, carefully washed with D.W., and then left dry in the laboratory at 27 °C for 24 h to remove the remaining moisture. Following the

grinding, 200 milliliters of D.W. were mixed with ten grams of ground powder in the beaker. The mixture was stirred at 150 rpm and heated to 70 °C for two hours. After allowing the extract to cool, it was filtered through filter paper Whatman No.1, yielding a pale-yellow extract that was subsequently refrigerated. This extract was reserved for future use in the production of the nanoparticles [37].

2.3. Synthesis of Adsorbent CuO NPs

The copper chloride dihydrate, $CuCl_2 \cdot 2H_2O$, and *Melia azedarach* fruit extract were used to create the nanoparticles. With constant stirring and heating at 60 °C, 50 mL of (0.1 M) $CuCl_2 \cdot 2H_2O$ solution was gradually added to (75 mL) of *Melia azedarach* fruit extract in the beaker. The formed CuO NPs were detected in the solution through UV–vis spectra (Figure 1) by changing in color from blue to viscous green. After 24 h of incubation, the sticky precipitate was subjected to centrifugation for 10 min at 10,000 rpm, followed by three to four rinses with deionized water. Upon drying the precipitate at room temperature for 48 h, a pellet was formed. The ultimate product underwent a 2 h calcination process at 400 °C in a muffle furnace after being dried to eliminate plant-derived organic substances. Then, it was powdered and preserved for further usage [12].

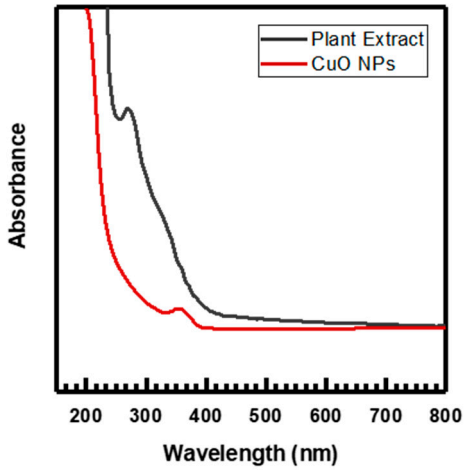

Figure 1. UV–visible spectra of plant extract and CuO NPs.

2.4. Characterization of CuO NPs

A spectrophotometer (Shimadzu UV–vis V-530A with a wavelength of 200 to 800 nm) was employed to determine the UV–vis absorption spectra of various substances. The synthesized CuO NPs were characterized using several techniques: field emission scanning electron microscopy (FE-SEM) in conjunction with X-ray energy-dispersive spectroscopy (EDS), Fourier transform infrared spectroscopy (FTIR), and X-ray diffraction (XRD). The morphology of CuO NPs was investigated using the QuantaTM 450 FEG. A SHIMADZU-IR PRESTIGE-21 Spectrometer was used to identify the functional groups of the CuO NPs. Using Bruker D8 Advance X-ray diffractometer (λ = 1.54 Å, 40 mA, 45 kV) and Cu-Kα radiation, the crystal structure of the CuO NPs was estimated throughout a 20–80° range.

2.5. Adsorption Batch Studies

The MB dye's optimal adsorption performance was achieved by adjusting the CuO NPs dose, contact time, and MB dye concentrations. After combining a weighed sample of CuO NPs with 3.0 milliliters of MB dye solution, the mixture's pH was adjusted. The mixture was stirred at a steady temperature before centrifugation at 150 rpm for a specific duration. By using the JANEWAY 7315 Spectrophotometer (with λmax of 660 nm), the amount of MB dye in the supernatant was determined. Equations (1) and (2) were used to

compute MB adsorption capacity (q) at equilibrium and at time, while Equation (3) was used for computing the dye removal percentage (%R) [38,39].

$$q_e = \frac{(C_i - C_e) * V}{M} \quad (1)$$

$$q_t = \frac{(C_i - C_t) * V}{M} \quad (2)$$

$$\%R = \frac{C_i - C_e}{C_i} \times 100 \quad (3)$$

where C_i, C_e, and C_t denote the MB dye concentration in the initial, at the equilibrium, and at time t (measured in milligrams per liter), respectively. V represents the solution volume in liters. Meanwhile, M refers to the mass of the CuO NPs adsorbent in grams.

2.6. Adsorption Kinetics and Isotherms Studies

The kinetics of adsorption provides useful data for adsorption process performance and design which can be applied practically. An investigation was conducted to examine the adsorption mechanism utilizing pseudo-first-order Equation (4), pseudo-second-order Equation (5), and Elovich Equation (6) for kinetic models [40,41].

$$log(q_e - q_t) = log q_e - \left(\frac{k_1}{2.303}\right) t \quad (4)$$

$$\frac{t}{q_t} = \frac{1}{k_2\ q_e^2} + \frac{1}{q_e}(t) \quad (5)$$

$$q_t = \frac{1}{\beta} ln\ (\alpha\beta) + \frac{1}{\beta} ln\ (t) \quad (6)$$

where t is the time, k_1 (min^{-1}), k_2 (g·mg^{-1} min^{-1}) are the rate constants for the pseudo-first-order and the pseudo-second-order models, respectively, α (mg·g^{-1}) is the rate of adsorption at initial, and β is the constant of desorption (g·mg^{-1}).

Adsorption isotherms can be used to examine the relationship between C_e and q_e of MB at a certain temperature. The adsorption isothermal behavior for CuO NPs was described using three models: Langmuir Equation (7), Freundlich Equation (8), and Tempkin Equation (9) [42,43].

$$\frac{1}{q_e} = \left(\frac{1}{k_L\ Q_m}\right)\frac{1}{C_e} + \frac{1}{Q_m} \quad (7)$$

$$log\ q_e = log\ K_f + \frac{1}{n} log\ C_e \quad (8)$$

$$q_e = B_T ln\ A_T + B_T\ lnC_e \quad (9)$$

where Q_m (mg·g^{-1}) is the maximum monolayer capacity, K_L (L·mg^{-1}), K_f (L.g^{-1}), and A_T (L·mg^{-1}) are the equilibrium rate constants for Langmuir, Freundlich, and Tempkin, respectively; $1/n$ represents an empirical constant indicating the adsorption intensity; $1/n$ is a constant indicating the adsorption intensity.

3. Results and Discussion

3.1. Characterization of CuO NPs

3.1.1. UV–Visible Adsorption Spectrum

The absorption spectrum of CuO NPs and *Melia azedarach* fruit extract in the UV–vis range has been depicted in Figure 1. The presence of various bioactive compounds, including flavonoids, alkaloids, carbohydrates, tannins, phenolic acid, and terpenoids, in the aqueous fruit extract of *Melia azedarach* has been attributed to the significant absorption peak observed at 269 nm. These compounds have been identified as being essential for

CuO NPs production [36,44]. CuO NPs production was shown by the fruit extract's quick color change to green upon the addition of $CuCl_2 \cdot 2H_2O$ solution. The confirmation of the reduction to CuO NPs was established through the observation of a significant absorption peak at 350 nm. This peak is probably connected to the CuO semiconductor excitation's surface plasmon resonance (SPR) [27,45,46].

3.1.2. FE-SEM and EDS

The size and shape of the synthesized CuO NPs were analyzed using FE-SEM micrographs. The FE-SEM micrographs of CuONPs before and after adsorption of MB dye are displayed in the inset of Figure 2a,b; these were captured at a resolution of 500 nm. Based on the FE-SEM image in Figure 2a, the produced CuO NPs displayed a uniform and distinctly spherical structure, though they exhibited some agglomeration due to the adhesive properties of the plant extract [47]. After adsorption, as shown in Figure 2b, the surface coverage of the CuO NPs is visible. This coverage is attributed to the adsorption of adsorbate molecules (MB), which is likely what leads to the formation of a monolayer of adsorbate molecules on the adsorbent surface. Image J software (1.48v) was used to measure the particle size of CuO NPs, as shown in Figure 2c. The results showed a particle size range between 20 and 40 nm, indicating the presence of well-established synthetic nanoparticles [48].

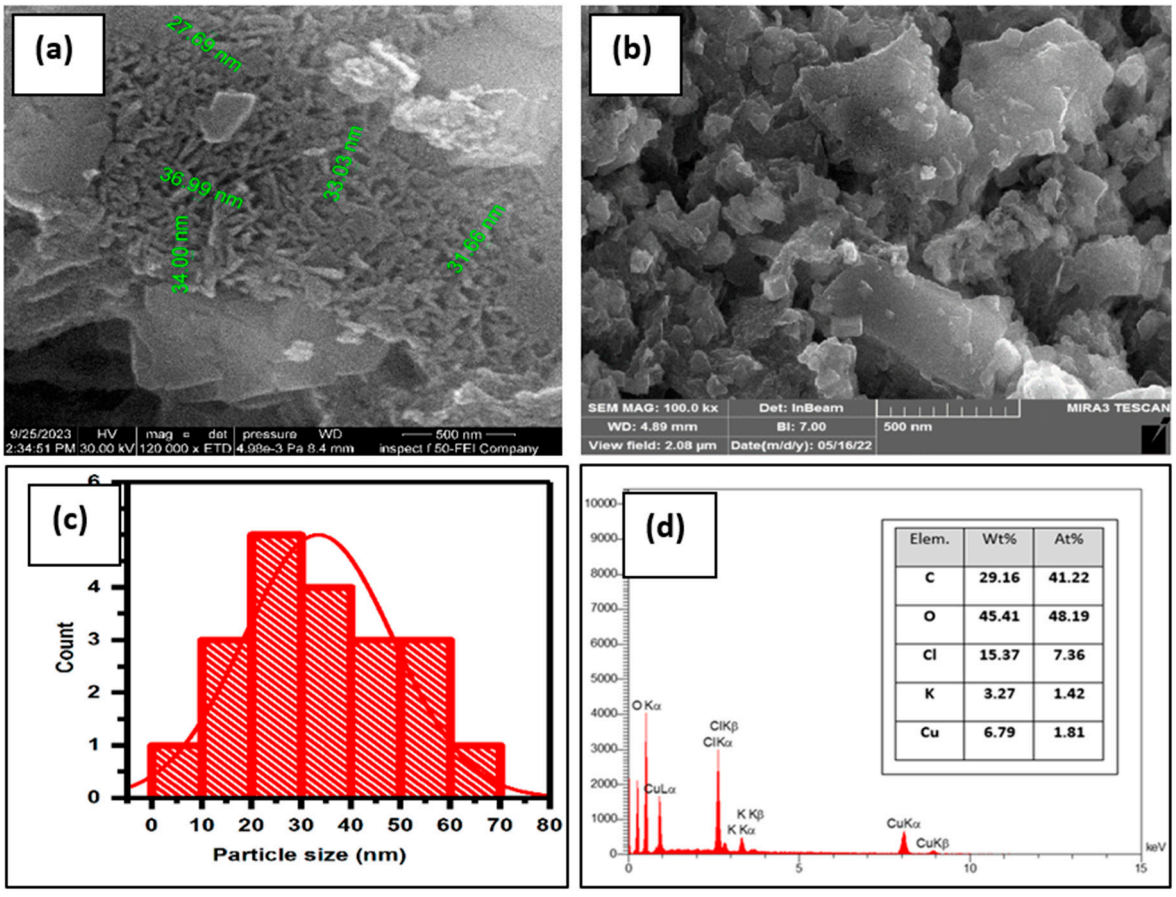

Figure 2. (**a**,**b**) FE-SEM analysis micrograph, (**c**) histogram, and (**d**) EDS of CuO NPs.

Additionally, the purity of the synthesized CuO NPs was demonstrated by an EDS spectrum, which was employed to evaluate the elemental analysis, as shown in Figure 2d. The presence of oxygen and copper in the EDS spectrum suggests that the copper is likely in the form of an oxide or dioxide. Copper (Cu) and oxygen (O) had weight compositions of 6.79 and 45.41 percent, respectively. Subsequently, the atomic compositions were de-

termined to be 1.81 percent and 48.19 percent, respectively. Due to interactions with the extract during the bioprocessing, minor amounts of carbon, chloride, and potassium were found. It was confirmed that CuO NPs were precisely created using green synthesis based on the SEM and EDS micrographs [49].

3.1.3. FTIR Spectroscopy

FTIR spectroscopy was utilized to investigate the various functional groups present in the synthesized CuO NPs within the spectral range of 400–4000 cm^{-1}, as shown in Figure 3a. The presence of phenolic compounds and absorbed water on the surface of CuO NPs is suggested by the bandwidth at (3524 cm^{-1}), which is associated with the -OH group stretching frequency [50]. Elevated peaks at (2922 cm^{-1} and 2865 cm^{-1}) indicate asymmetric stretching of C-H bonds in $-CH_2$ and $-CH_3$ groups, respectively [31,51].

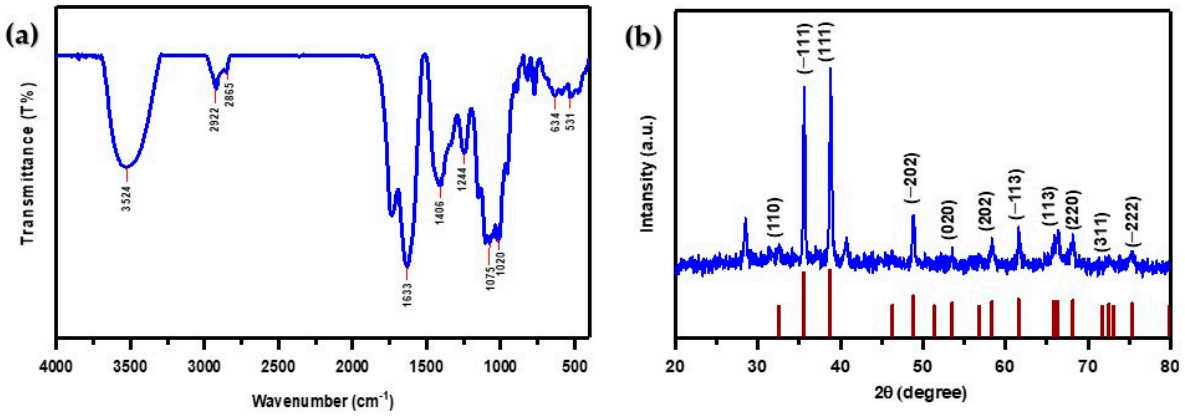

Figure 3. (**a**) FTIR spectra of CuO NPs; (**b**) XRD pattern of CuO NPs.

The C=C aromatic bending vibration of alkenes in the *Melia azedarach* fruit extract is responsible for the strong absorption band that appeared at (1633 cm^{-1}) [52,53]. The deformation vibration of the alkane group's C–H band is responsible for the sharp peak at (1406 cm^{-1}). The presence of various organic functional groups such as ethers, amides, and other aliphatic groups on the surface of CuO NPs is demonstrated by the peaks observed at (1244 cm^{-1} and 1075 cm^{-1}). The absorption peak observed in primary and secondary alcohols at (1020 cm^{-1}) is due to the stretching vibration of the C-O group [54].

Furthermore, Cu-O vibrations can be linked to peaks at (531 cm^{-1} and 634 cm^{-1}), demonstrating the production of CuO nanoparticles [52,55]. The bioactive compounds present in *Melia azedarach* fruit extract have a significant impact on the production of CuO NPs. The FTIR analysis showed that the synthesized CuO NPs have many functional groups. These groups are most reactive to adsorbing MB dye cations through an electrostatic interaction [56].

3.1.4. XRD

Figure 3b illustrates the X-ray diffraction pattern of CuO NPs, prepared using the green synthesis technique involving *Melia azedarach* fruit extract. The prominent reflection planes correspond to (110), (−111), (111), (−202), (020), (202), (−113), (113), (220), (311), and (−222), with associated scattering angles of 32.54°, 35.56°, 38.77°, 48.74°, 53.53°, 58.37°, 61.56°, 67.98°, 68.17°, 72.49°, and 75.29°, respectively. The presence of sharpened and well-defined scattering peaks serves as strong evidence supporting the crystalline nature of the CuO nanoparticles, indicating their purity without impurities. The obtained diffraction data closely matched the information recorded in the JCPDS card no. 801268 [57,58].

3.2. Batch Adsorption Studies

3.2.1. Effect of pH

The CuO NP adsorption efficiency was examined in MB dye solutions at a concentration (10 mg·L^{-1}) and a pH (4 to 8). Figure 4 shows that both the percentage of removal %*R* and the adsorption capacity (q_e) of MB significantly improved when the pH value was raised from 4 to 8. Adsorption sites that are positively charged and open the uptake of anions found in solutions with low pH values. The competitiveness of H^+ ions and dye cations for the few available adsorption sites may be the cause of the reduced MB adsorption at acidic pH values. The maximum MB adsorption percentage %*R* was 82.051% at a pH of 8. For the next experiments, pH 8 was chosen because of this. In general, these results are compatible with previous studies [4,59,60].

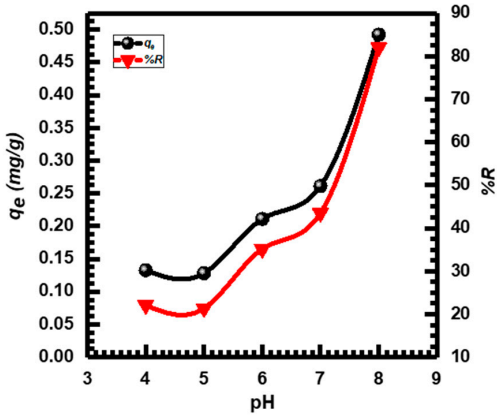

Figure 4. pH effect on MB adsorption by CuO NPs.

3.2.2. Effect of CuO NPs Dose

The utilized amount of CuO NPs adsorbent had a considerable impact on the effectiveness of adsorption. CuO NPs adsorbent doses ranging from 0.01 to 0.09 g were employed to investigate the adsorption of MB dye [61,62]. Figure 5 depicts the effects of adsorbent dose on MB adsorption. The typical pattern of quickly rising %*R* as the adsorbent dose increased was followed and equilibrium was attained at 0.09 g with a maximum %*R* of 93.800%. This was associated with a rise in adsorption-active sites with an increase in dosage, both the adsorbent outer layer and the expanded adsorption sites number, leading to enhanced efficiency in %*R*. However, the q_e value decreased with increasing the adsorbent dose. The existence of more active sites on the surface of CuO NPs may be the cause of the observed drop in adsorption (q_e) when doses were high, and the ensuing decrease in accessible MB molecules for adsorption [17,63]. Consequently, 0.05 g of CuO NPs was chosen for subsequent studies based on the findings of the dose experiment.

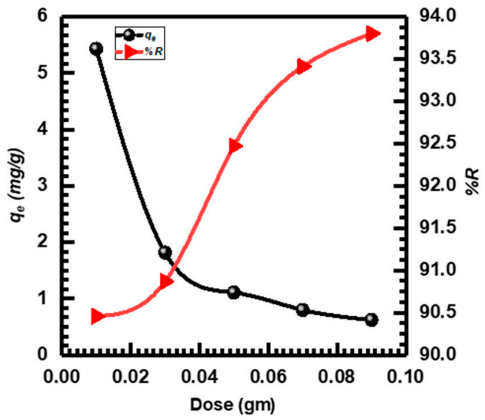

Figure 5. CuO NPs dose adsorbent effect on MB adsorption.

3.3. Effect of Contact Time and Kinetic Study

Figure 6a displays the UV–vis spectra of the MB absorption at various times (5–120 min) after being adsorbed by the CuO NPs. The uniqueness of the adsorption process is evident from the consistent decrease in absorbance intensity without any changes in wavelength throughout the adsorption [7,64].

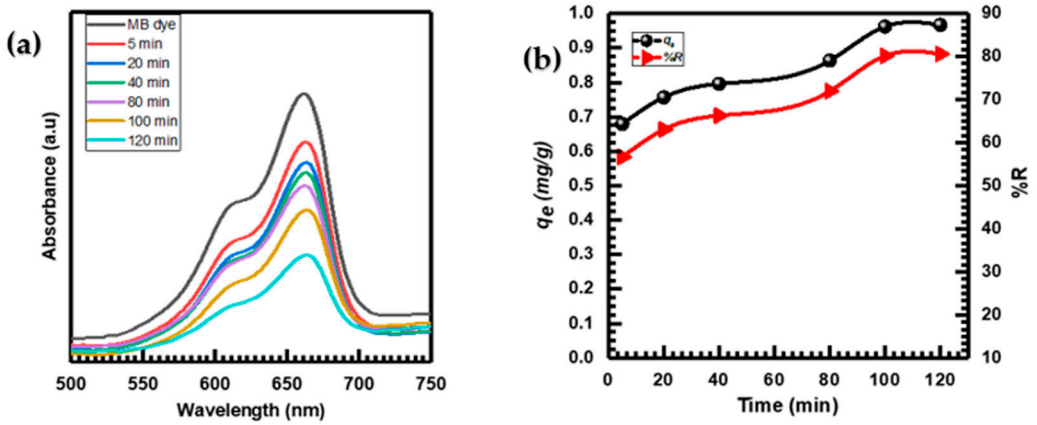

Figure 6. (**a**) UV–vis spectra of MB adsorption by CuO NPs at different times; (**b**) contact time effect on MB adsorption.

Figure 6b illustrates the effects of time on MB adsorption onto CuO NPs. As the adsorption duration increased, the MB's adsorption capacity (q_e) and removal percentage %R both rose until they reached equilibrium after 120 min. At equilibrium, the q_e for MB was established to be 0.96 (mg·g^{-1}), while the corresponding %R was determined to be 80.598% [65].

Experimental data from batch studies were fitted with the pseudo-first-order Figure 7a, pseudo-second-order Figure 7b, and Elovich Figure 7c kinetic models to assess the adsorption kinetics of MB under the optimal adsorption conditions and provide additional insight into the features of the adsorption process [2,5,66]. Kinetic parameter results for these three models are listed in Table 1.

Table 1. Kinetic parameters result from the adsorption of MB onto CuO NPs.

Pseudo-First-Order Parameters				**Pseudo-Second-Order Parameters**				**Elovich Parameters**		
K_1	$(q_e)_{exp.}$	$(q_e)_{calc.}$	R^2	K_2	$(q_e)_{exp.}$	$(q_e)_{calc.}$	R^2	α	β	R^2
0.0345	0.9723	0.5151	0.8533	0.1562	0.9723	0.9971	0.9925	25.5379	11.1359	0.8944

According to the data presented (Table 1), the correlation coefficient R^2 value of the pseudo-second-order kinetic model (0.9925) is much higher than that of the pseudo-first-order (0.8533) and Elovich (0.8944) kinetic models. This indicated that the pseudo-second-order model provided a more precise description of the adsorption kinetics of MB [67]. Additionally, there was a high level of agreement between the experimental value $(q_e)_{exp.}$ (0.9723) and the calculated value $(q_e)_{calc.}$ (0.9971) for the pseudo-second-order kinetic model. This finding serves as evidence of the precision of the model [68]. As compared to other models, the pseudo-second-order kinetic model exhibited better performance in removing MB dye from solutions using CuO NPs [38,69,70].

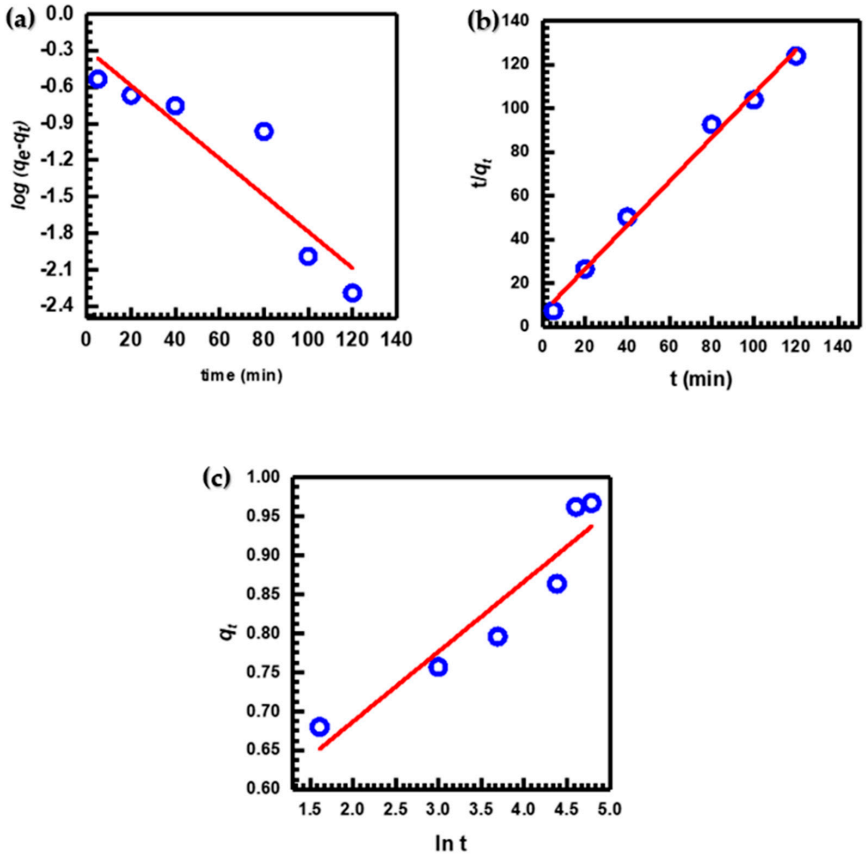

Figure 7. (**a**) Pseudo-first-order, (**b**) pseudo-second-order, and (**c**) Elovich kinetic models for MB adsorption.

3.4. Effect of Initial Concentration and Isotherms Study

Figure 8 shows that CuO NPs' adsorption capacity (q_e) and removal percentage (%R) are significantly influenced by the initial MB concentration (C_i). When the C_i increased, the %R remained constant from 81.026% to 85.869%, while the q_e values of the CuO NPs increased by 0.498, 0.972, 1.546, 2.027, and 2.497 mg·g^{-1} for concentrations of 10, 20, 30, 40, and 50 mg·L^{-1}, respectively. This can be attributed as the C_i increased, the resistance to MB mass transferring across solid phases and aqueous phases is overcome, resulting in increased sorption. Furthermore, when the MB concentration rose, the interaction between MB and the CuO NPs was enhanced, accelerating the sorption process [71,72]. Other studies conducted by different researchers have reported comparable findings concerning the influence of the initial MB concentration [73,74].

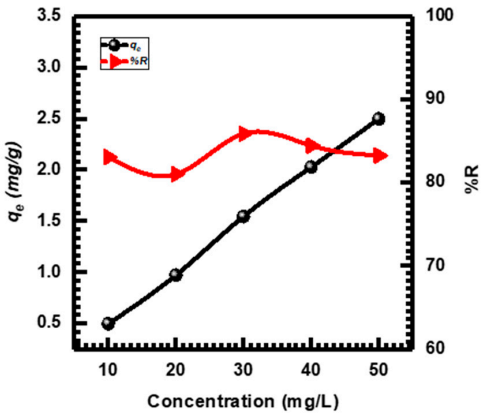

Figure 8. Different concentrations affect MB adsorption.

An adsorption isotherm describes the distribution of adsorbate molecules between the liquid and solid phases once the adsorption process has reached equilibrium. In cases where the adsorption surface is homogeneous and the affinity of the adsorbate is the same at each adsorption site, the Langmuir isotherm is often the most appropriate model to use [75]. The Freundlich isotherm model was developed specifically for heterogeneous systems and describes multilayer adsorption occurring on the sorbent surface [76]. According to the Temkin isotherm, as adsorbate coverage increases, the heat of adsorption of each molecule in the layer drops linearly [77]. Figure 9a–c depicts the linear models used to study the interactions of MB on the CuO NP surface. Table 2 displays the computed values of the parameters in the Langmuir, Freundlich, and Tempkin equations.

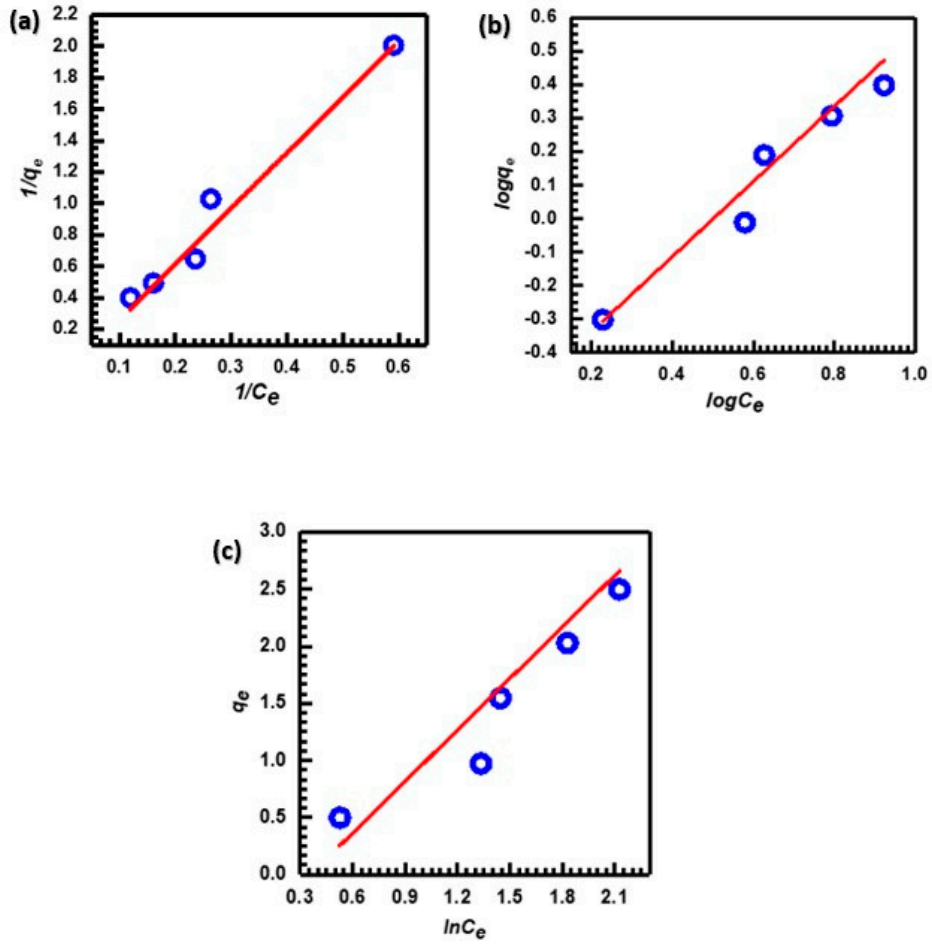

Figure 9. (**a**) Langmuir, (**b**) Freundlich, and (**c**) Tempkin adsorption isotherms for adsorption of MB.

Table 2. Results of the adsorption isotherms parameters for MB adsorption onto CuO NPs.

Langmuir Parameters			Freundlich Parameters			Tempkin Parameters			
K_L	Q_m	R^2	Kf	n	R^2	A_T	B_T	b_T	R^2
0.011	26.738	0.9754	3.475	1.042	0.9603	1.2997	1.2680	1953.921	0.9225

After examining the data in Table 2, the Langmuir isotherm model was found to have a significantly higher correlation coefficient (R^2 = 0.9754) with the adsorption of MB by CuO NPs compared to other isotherm models. This value proves that the parameter and the confirmation of monolayer adsorption of MB onto CuO NPs are in good agreement [78]. The value of Q_m indicates how much MB dye is needed for every unit weight of sorbent to form a full monolayer on the CuO NPs surface. Table 3 shows the CuO NPs' adsorption

capacity Q_m for MB dye adsorption compared to different types of adsorbents in the previous studies.

Table 3. The adsorption capacities Q_m for different types of MB adsorbents in the previous studies.

Adsorbent Material	Q_m	Time	pH	[Ref.]
Synthesized CuO-A NPs	95.5	180 min.	>10	[79]
Biochar-TiO_2	74.30	60 min	6.0	[80]
Lignite Coal	40.82	60 min.	6.35	[73]
Nanoparticles of microalgae	58.82	180 min.	6.0	[81]
La-Na Co-Doped TiO_2 NPs	25.04	25 min.	7.0	[82]
CuO NPs	26.73	120 min.	8.0	This study
Cu-NPs/Centaurea cyanus Plant	21.9	101.5 min	6.6	[83]
synthesized -$NiMoO_4$ nano sorbents	16.86	120 min.	11	[63]
NiO	10.58	150 min.	6.5	[84]
Silica nano-sheets	9.7	180 min.	7.0	[85]
Fly ash	5.71	60 min.	8.0	[86]

Additionally, the Freundlich isotherm's n value provides a clear indication of the adsorption behavior. Generally, the adsorption is classified as (i) chemical, (ii) physical, or (iii) linear depending on whether n is less than, greater than, or equal to one [87,88]. Physical adsorption outperforms chemical adsorption in the case of CuO NPs since the value of n is greater than one (1.042). Furthermore, the value of $1/n$ (0.960) falls within the range $0 < 1/n < 1$, demonstrating that the adsorption process is favorable [89]. The adsorption of dyes involves numerous mechanisms, including ion exchange, hydrogen bonding, Van der Waals forces, electrostatics, and dipole–ion interaction. According to the kinetic and isotherm data, the adsorption mechanism of MB onto CuO NPs is mainly based on physical attraction. Therefore, it can be suggested that electrostatic interactions are the main mechanism of adsorption [90].

4. Conclusions

It can be concluded that the aqueous extract from *Melia azedarach* fruit was successfully used to synthesize CuO NPs utilizing the green route approach. The bioactive compounds in *Melia azedarach*'s aqueous fruit extract can serve as a reducing agent to synthesize the CuO NPs. The prepared particles were spherical in morphology and ranged in size from 20 to 40 nm on average. According to the results, CuO nanoparticles show great promise for successfully removing MB dye from aqueous solutions. The optimum conditions for the elimination of MB dye were pH (8), adsorbent dosage (0.05 g), initial MB concentration (20 $mg{\cdot}L^{-1}$), and a period of 120 min. The pseudo-second-order kinetic model accurately described the adsorption process. Furthermore, the values of the calculated adsorption capacity $(q_e)_{calc.}$ (0.9971) and the experimental adsorption capacity $(q_e)_{exp.}$ (0.9723) exhibits good agreement. The Langmuir isotherm offered a good fit to the data and the maximum adsorption capacity toward MB was 26.738 $mg{\cdot}g^{-1}$.

Funding: This research received no external funding.

Data Availability Statement: The data presented in this study are available in the article.

Acknowledgments: The author expresses gratitude to Suhad A. Yasin, the P.I to the USAID Partnerships for the Enhanced Engagement in Research (PEER) Program-Iraq-cycle 6, for her constant support throughout the research work.

Conflicts of Interest: The author declares no conflicts of interest.

References

1. Kuang, Y.; Zhang, X.; Zhou, S. Adsorption of Methylene Blue in Water onto Activated Carbon by Surfactant Modification. *Water* **2020**, *12*, 587. [CrossRef]
2. Viscusi, G.; Lamberti, E.; Gorrasi, G. Design of a hybrid bio-adsorbent based on Sodium Alginate/Halloysite/Hemp hurd for methylene blue dye removal: Kinetic studies and mathematical modeling. *Colloids Surf.* **2022**, *633*, 127925. [CrossRef]
3. Jabbar, K.Q.; Barzinjy, A.A.; Hamad, S.M. Iron oxide nanoparticles: Preparation methods, functions, adsorption and coagulation/flocculation in wastewater treatment. *Environ. Nanotechnol. Monit. Manag.* **2022**, *17*, 100661. [CrossRef]
4. Essa, W.K.; Yasin, S.A.; Abdullah, A.H.; Thalji, M.R.; Saeed, I.A.; Assiri, M.A.; Chong, K.F.; Ali, G.A.M. Taguchi L25 (54) Approach for Methylene Blue Removal by Polyethylene Terephthalate Nanofiber-Multi-Walled Carbon Nanotube Composite. *Water* **2022**, *14*, 1242. [CrossRef]
5. Selim, M.T.; Salem, S.S.; Mohamed, A.A.; El-Gamal, M.S.; Awad, M.F.; Fouda, A. Biological Treatment of Real Textile Effluent Using *Aspergillus flavus* and *Fusarium oxysporium* and Their Consortium along with the Evaluation of Their Phytotoxicity. *J. Fungi* **2021**, *7*, 193. [CrossRef]
6. Song, S.; Fan, J.; He, Z.; Zhan, L.; Liu, Z.; Chen, J.; Xu, X. Electrochemical degradation of azo dye C.I. Reactive Red 195 by anodic oxidation on Ti/SnO_2–Sb/PbO_2 electrodes. *Electrochim. Acta* **2010**, *55*, 3606–3613. [CrossRef]
7. Laouini, S.E.; Bouafia, A.; Soldatov, A.V.; Algarni, H.; Tedjani, M.L.; Ali, G.A.M.; Barhoum, A. Green Synthesized of Ag/Ag_2O Nanoparticles Using Aqueous Leaves Extracts of *Phoenix dactylifera* L. and Their Azo Dye Photodegradation. *Membranes* **2021**, *11*, 468. [CrossRef]
8. Zhao, J.; Dang, Z.; Muddassir, M.; Raza, S.; Zhong, A.; Wang, X.; Jin, J. A new Cd (II)-based coordination polymer for efficient photocatalytic removal of organic dyes. *Molecules* **2023**, *28*, 6848. [CrossRef]
9. Dong, X.; Li, Y.; Li, D.; Liao, D.; Qin, T.; Prakash, O.; Kumar, A.; Liu, J. A new 3D 8-connected Cd (ii) MOF as a potent photocatalyst for oxytetracycline antibiotic degradation. *CrystEngComm* **2022**, *24*, 6933–6943. [CrossRef]
10. Ramesh, A.V.; Rama Devi, D.; Mohan Botsa, S.; Basavaiah, K. Facile green synthesis of Fe_3O_4 nanoparticles using aqueous leaf extract of *Zanthoxylum armatum* DC. for efficient adsorption of methylene blue. *J. Asian Ceram. Soc.* **2018**, *6*, 145–155. [CrossRef]
11. Mustapha, S.; Ndamitso, M.M.; Abdulkareem, A.S.; Tijani, J.O.; Shuaib, D.T.; Ajala, A.O.; Mohammed, A.K. Application of TiO_2 and ZnO nanoparticles immobilized on clay in wastewater treatment: A review. *Appl. Water Sci.* **2020**, *10*, 49. [CrossRef]
12. Yasin, S.A.; Zeebaree, S.Y.S.; Zeebaree, A.Y.S.; Zebari, O.I.H.; Saeed, I.A. The efficient removal of methylene blue dye using CuO/PET nanocomposite in Aqueous solutions. *Catalysts* **2021**, *11*, 241. [CrossRef]
13. Sone, B.T.; Diallo, A.; Fuku, X.G.; Gurib-Fakim, A.; Maaza, M. Biosynthesized CuO nano-platelets: Physical properties & enhanced thermal conductivity nanofluidics. *Arab. J. Chem.* **2020**, *13*, 160–170. [CrossRef]
14. Maqbool, Q.; Iftikhar, S.; Nazar, M.; Abbas, F.; Saleem, A.; Hussain, T.; Kausar, R.; Anwaar, S.; Jabeen, N. Green fabricated CuO nanobullets via Olea europaea leaf extract shows auspicious antimicrobial potential. *IET Nanobiotechnol.* **2017**, *11*, 463–468. [CrossRef] [PubMed]
15. Akintelu, S.A.; Folorunso, A.S.; Folorunso, F.A.; Oyebamiji, A.K. Green synthesis of copper oxide nanoparticles for biomedical application and environmental remediation. *Heliyon* **2020**, *6*, e04508. [CrossRef]
16. Silva, N.; Ramírez, S.; Díaz, I.; Garcia, A.; Hassan, N. Easy, Quick, and Reproducible Sonochemical Synthesis of CuO Nanoparticles. *Materials* **2019**, *12*, 804. [CrossRef] [PubMed]
17. Rangel, W.M.; Santa, R.A.A.B.; Riella, H.G. A facile method for synthesis of nanostructured copper (II) oxide by coprecipitation. *J. Mater. Res. Technol.* **2020**, *9*, 994–1004. [CrossRef]
18. Khashan, K.S.; Sulaiman, G.M.; Abdulameer, F.A. Synthesis and Antibacterial Activity of CuO Nanoparticles Suspension Induced by Laser Ablation in Liquid. *Arab. J. Sci. Eng.* **2016**, *41*, 301–310. [CrossRef]
19. Gounder Thangamani, J.; Khadheer Pasha, S.K. Hydrothermal synthesis of copper (II) oxide-nanoparticles with highly enhanced BTEX gas sensing performance using chemiresistive sensor. *Chemosphere* **2021**, *277*, 130237. [CrossRef]
20. Sivayogam, D.; Kartharinal Punithavathy, I.; Johnson Jayakumar, S.; Mahendran, N. Study on structural, electro-optical and optoelectronics properties of CuO nanoparticles synthesis via sol gel method. *Mater. Today Proc.* **2022**, *48*, 508–513. [CrossRef]
21. Devi, D.; Julkapli, N.M.; Sagadevan, S.; Johan, M.R. Eco-friendly green synthesis approach and evaluation of environmental and biological applications of Iron oxide nanoparticles. *Inorg. Chem. Commun.* **2023**, *152*, 110700. [CrossRef]
22. Chaudhary, J.; Tailor, G.; Yadav, M.; Mehta, C. Green route synthesis of metallic nanoparticles using various herbal extracts: A review. *Biocatal. Agric. Biotechnol.* **2023**, *50*, 102692. [CrossRef]
23. Waghchaure, R.H.; Adole, V.A. Biosynthesis of metal and metal oxide nanoparticles using various parts of plants for antibacterial, antifungal and anticancer activity: A review. *J. Indian Chem. Soc.* **2023**, *100*, 100987. [CrossRef]
24. Radulescu, D.-M.; Surdu, V.-A.; Ficai, A.; Ficai, D.; Grumezescu, A.-M.; Andronescu, E. Green synthesis of metal and metal oxide nanoparticles: A review of the principles and biomedical applications. *Int. J. Mol. Sci.* **2023**, *24*, 15397. [CrossRef] [PubMed]
25. Eid, A.M.; Fouda, A.; Hassan, S.E.-D.; Hamza, M.F.; Alharbi, N.K.; Elkelish, A.; Alharthi, A.; Salem, W.M. Plant-Based Copper Oxide Nanoparticles; Biosynthesis, Characterization, Antibacterial Activity, Tanning Wastewater Treatment, and Heavy Metals Sorption. *Catalysts* **2023**, *13*, 348. [CrossRef]
26. Phang, Y.-K.; Aminuzzaman, M.; Akhtaruzzaman, M.; Muhammad, G.; Ogawa, S.; Watanabe, A.; Tey, L.-H. Green synthesis and characterization of CuO nanoparticles derived from papaya peel extract for the photocatalytic degradation of palm oil mill effluent (POME). *Sustainability* **2021**, *13*, 796. [CrossRef]

27. Gebremedhn, K.; Kahsay, M.H.; Aklilu, M. Green Synthesis of CuO Nanoparticles Using Leaf Extract of Catha edulis and Its Antibacterial Activity. *J. Pharm. Pharmacol.* **2019**, *7*, 327–342. [CrossRef] [PubMed]
28. Berra, D.; Salah Eddine, L.; Boubaker, B.; Mohammed Ridha, O.; Berrani, D.; Achour, R. Green Synthesis of Copper Oxide Nanoparticles by Pheonix Dactylifera L Leaves Extract. *Dig. J. Nanomater. Biostruct.* **2018**, *13*, 1231–1238.
29. Chowdhury, R.; Khan, A.; Rashid, M.H. Green synthesis of CuO nanoparticles using Lantana camara flower extract and their potential catalytic activity towards the aza-Michael reaction. *RSC Adv.* **2020**, *10*, 14374–14385. [CrossRef]
30. Dulta, K.; Koşarsoy Ağçeli, G.; Chauhan, P.; Jasrotia, R.; Chauhan, P.K.; Ighalo, J.O. Multifunctional CuO nanoparticles with enhanced photocatalytic dye degradation and antibacterial activity. *Sustain. Environ. Res.* **2022**, *32*, 2. [CrossRef]
31. Alhalili, Z. Green synthesis of copper oxide nanoparticles CuO NPs from Eucalyptus Globoulus leaf extract: Adsorption and design of experiments. *Arab. J. Chem.* **2022**, *15*, 103739. [CrossRef]
32. Shammout, M.; Awwad, A. A novel route for the synthesis of copper oxide nanoparticles using Bougainvillea plant flowers extract and antifungal activity evaluation. *Chem. Int.* **2021**, *7*, 71–78. [CrossRef]
33. Feng, L.; Tian, X.; El-Kassaby, Y.A.; Qiu, J.; Feng, Z.; Sun, J.; Wang, G.; Wang, T. Predicting suitable habitats of *Melia azedarach* L. in China using data mining. *Sci. Rep.* **2022**, *12*, 12617. [CrossRef]
34. Idrees, Z.Z.; Mustafa, M.A. Effect of silver nanoparticles using *Melia azedarach* L. leaf extract on house fly *Musca domestica* L. *Int. J. Multidiscip. Res. Growth Eval.* **2021**, *2*, 44–48.
35. Rubae, A.A.-Y. The potential uses of *Melia azedarach* L. as pesticidal and medicinal plant, review. *Am. J. Sustain. Agric.* **2009**, *3*, 185–194.
36. Hassan, W.A.; Al-Doski, J.M.M.; Ebo, N.Y.M. Antimicrobial activity of chinaberry Melia azedarach extract against Pseudomonas syringae pv. syringae in vitro. *J. Duhok Univ.* **2018**, *21*, 29–36. [CrossRef]
37. Manokari, M.; Ravindran, C.P.; Shekhawat, M.S. Biosynthesis of zinc oxide nanoparticles using *Melia azedarach* L. extracts and their characterization. *Int. J. Pharm. Sci. Res.* **2016**, *1*, 31–36.
38. Mosoarca, G.; Popa, S.; Vancea, C.; Boran, S. Optimization, equilibrium and kinetic modeling of methylene blue removal from aqueous solutions using dry bean pods husks powder. *Materials* **2021**, *14*, 5673. [CrossRef]
39. Thamer, B.M.; Aldalbahi, A.; Moydeen, M.; El-Hamshary, H.; Al-Enizi, A.M.; El-Newehy, M.H. Effective adsorption of Coomassie brilliant blue dye using poly (phenylene diamine) grafted electrospun carbon nanofibers as a novel adsorbent. *Mater. Chem. Phys.* **2019**, *234*, 133–145. [CrossRef]
40. Wu, K.; Huang, W.; Hung, W.; Tsai, C. Modified expanded graphite/Fe_3O_4 composite as an adsorbent of methylene blue: Adsorption kinetics and isotherms. *Mater. Sci. Eng. B* **2021**, *266*, 115068. [CrossRef]
41. Ahmed, H.A.; Saleem, P.H.; Yasin, S.A.; Saeed, I.A. A kinetic study of removing methylene blue from aqueous solutions by modified electrospun polyethelene terephthalate nanofibres. *Egypt. J. Chem.* **2021**, *64*, 2803–2813. [CrossRef]
42. Alhasan, H.S.; Alahmadi, N.; Yasin, S.A.; Khalaf, M.Y.; Ali, G.A.M. Low-Cost and Eco-Friendly Hydroxyapatite Nanoparticles Derived from Eggshell Waste for Cephalexin Removal. *Separations* **2022**, *9*, 10. [CrossRef]
43. Rojas, J.; Suarez, D.; Moreno, A.; Silva-Agredo, J.; Torres-Palma, R.A. Kinetics, isotherms and thermodynamic modeling of liquid phase adsorption of crystal violet dye onto Shrimp-Waste in its raw, pyrolyzed material and activated charcoals. *Appl. Sci.* **2019**, *9*, 5337. [CrossRef]
44. Leaves, E.P. Characterization of ZnO Nanoparticles Prepared from Green Synthesis Using EAJSE Characterization of ZnO Nanoparticles Prepared from Green Synthesis Using Euphorbia Petiolata Leaves. *Eurasian J. Sci. Eng.* **2019**, *4*, 74–83. [CrossRef]
45. Buazar, F.; Badri, M. Biofabrication of highly pure copper oxide nanoparticles using wheat seed extract and A mechanistic approach. *Green Process. Synth.* **2019**, *8*, 691–702. [CrossRef]
46. Yasin, S.A.; Abbas, J.A.; Saeed, I.A.; Ahmed, I.H. The application of green synthesis of metal oxide nanoparticles embedded in polyethylene terephthalate nanofibers in the study of the photocatalytic degradation of methylene blue. *Polym. Bull.* **2020**, *77*, 3473–3484. [CrossRef]
47. Kumari, V.; Kaushal, S.; Singh, P.P. Green synthesis of a CuO/rGO nanocomposite using a *Terminalia arjuna* bark extract and its catalytic activity for the purification of water. *Mater. Adv.* **2022**, *3*, 2170–2184. [CrossRef]
48. Mustafa, G.; Tahir, H.; Sultan, M.; Akhtar, N. Synthesis and characterization of cupric oxide (CuO) nanoparticles and their application for the removal of dyes. *Afr. J. Biotechnol.* **2013**, *12*, 6650–6660. [CrossRef]
49. Raj, S.; Trivedi, R. Biosynthesis of copper oxide nanoparticles using *Enicostemma axillare* (*Lam.*) leaf extract. *Biochem. Biophys. Rep.* **2019**, *20*, 100699. [CrossRef]
50. Gowri, M.; Latha, N.; Rajan, M. Copper Oxide Nanoparticles Synthesized Using *Eupatorium odoratum*, *Acanthospermum hispidum* Leaf extracts, and Its Antibacterial Effects Against Pathogens: A Comparative Study. *Bionanoscience* **2019**, *9*, 545–552. [CrossRef]
51. Pansambal, S.; Gavande, S.; Ghotekar, S.; Oza, R.; Deshmukh, K. Green Synthesis of CuO Nanoparticles using *Ziziphus mauritiana* L. Extract and Its Characterizations. *Int. J. Sci. Res. Sci. Technol.* **2018**, *3*, 1388–1392. [CrossRef]
52. Saif, S.; Tahir, A.; Asim, T.; Chen, Y. Plant Mediated Green Synthesis of CuO Nanoparticles: Comparison of Toxicity of Engineered and Plant Mediated CuO Nanoparticles towards *Daphnia magna*. *Nanomaterials* **2016**, *6*, 205. [CrossRef] [PubMed]
53. Sundar, S.; Venkatachalam, G. Biosynthesis of Copper Oxide (CuO) Nanowires and Their Use for the Electrochemical Sensing of Dopamine. *Nanomaterials* **2018**, *8*, 823. [CrossRef] [PubMed]
54. Veisi, H.; Karmakar, B.; Tamoradi, T.; Hemmati, S.; Hekmati, M. Biosynthesis of CuO nanoparticles using aqueous extract of herbal tea (*Stachys lavandulifolia*) flowers and evaluation of its catalytic activity. *Sci. Rep.* **2021**, *11*, 1983. [CrossRef]

55. Aminuzzaman, M.; Kei, L.M.; Liang, W.H. Green Synthesis of Copper Oxide (CuO) Nanoparticles using Banana Peel Extract and Their Photocatalytic Activities. *AIP Conf. Proc.* **2017**, *1828*, 020016. [CrossRef]
56. Wang, W.; Xia, Z.; Tian, Z.; Jiang, H.; Zhan, Y.; Liu, C.; Li, C.; Zhou, H. Chemical constituents from the fruits of *Melia azedarach* (Meliaceae). *Biochem. Syst. Ecol.* **2020**, *92*, 104094. [CrossRef]
57. Eslami, A.; Juibari, N.M.; Hosseini, S.G.; Abbasi, M. Synthesis and characterization of CuO nanoparticles by the chemical liquid deposition method and investigation of its catalytic effect on the thermal decomposition of ammonium perchlorate. *Cent. Eur. J. Energetic Mater.* **2017**, *14*, 152–168. Available online: http://yadda.icm.edu.pl/baztech/element/bwmeta1.element.baztech-6a824ec1-d219-44a4-a0e1-4bd7ee120a9f (accessed on 17 January 2024). [CrossRef]
58. Shi, L.-B.; Tang, P.-F.; Zhang, W.; Zhao, Y.-P.; Zhang, L.-C.; Zhang, H. Green synthesis of CuO nanoparticles using *Cassia auriculata* leaf extract and in vitro evaluation of their biocompatibility with rheumatoid arthritis macrophages (RAW 264.7). *Trop. J. Pharm. Res.* **2017**, *16*, 185–192. [CrossRef]
59. Karami, K.; Beram, S.M.; Bayat, P.; Siadatnasab, F. A novel nanohybrid based on metal—Organic framework MIL101—Cr/PANI/Ag for the adsorption of cationic methylene blue dye from aqueous solution. *J. Mol. Struct.* **2022**, *1247*, 131352. [CrossRef]
60. Goharrizi, A.S.; Azadi, M.; Shahryari, Z. Experimental study of methylene blue adsorption from aqueous solutions onto carbon nano tubes. *Int. J. Water Resour. Environ. Eng.* **2010**, *2*, 16–028.
61. Wanga, Z.; Pan Hanb, Y.J.; Mab, D.; Doub, C.; Hanb, R. Adsorption of congo red using ethylenediamine modified wheat straw. *Desalin. Water Treat.* **2011**, *30*, 37–41. [CrossRef]
62. Que, W.; Jiang, L.; Wang, C.; Liu, Y.; Zeng, Z.; Wang, X.; Ning, Q.; Liu, S.; Zhang, P.; Liu, S. Influence of sodium dodecyl sulfate coating on 3 adsorption of methylene blue by biochar from 4 aqueous solution. *J. Environ. Sci.* **2017**, *70*, 166–174. [CrossRef]
63. Rakass, S.; Oudghiri Hassani, H.; Mohmoud, A.; Kooli, F.; Abboudi, M.; Assirey, E.; Al Wadaani, F. Highly efficient methylene blue dye removal by nickel molybdate nanosorbent. *Molecules* **2021**, *26*, 1378. [CrossRef] [PubMed]
64. Dinh, V.; Huynh, T.; Le, H.M.; Nguyen, V. Insight into the adsorption mechanisms of methylene blue and chromium(III) from aqueous solution onto pomelo fruit peel. *RSC Adv.* **2019**, *9*, 25847–25860. [CrossRef] [PubMed]
65. Liu, L.; Fan, S.; Li, Y. Removal Behavior of Methylene Blue from Aqueous Solution by Tea Waste: Kinetics, Isotherms and Mechanism. *Int. J. Environ. Res. Public Health* **2018**, *15*, 1321. [CrossRef] [PubMed]
66. Nizam, N.U.M.; Hanafiah, M.M.; Mahmoudi, E.; Halim, A.A.; Mohammad, A.W. The removal of anionic and cationic dyes from an aqueous solution using biomass-based activated carbon. *Sci. Rep.* **2021**, *11*, 8623. [CrossRef]
67. Berkane, N.; Meziane, S.; Aziri, S. Optimization of Congo red removal from aqueous solution using Taguchi experimental design. *Sep. Sci. Technol.* **2020**, *55*, 278–288. [CrossRef]
68. Abbas, J.A.; Said, I.A.; Mohamed, M.A.; Yasin, S.A.; Ali, Z.A.; Ahmed, I.H. Electrospinning of polyethylene terephthalate (PET) nanofibers: Optimization study using taguchi design of experiment. In Proceedings of the IOP Conference Series: Materials Science and Engineering, Bangkok, Thailand, 24–26 February 2018; IOP Publishing: Bristol, UK, 2018; Volume 454, p. 12130.
69. Cheng, J.; Zhan, C.; Wu, J.; Cui, Z.; Si, J.; Wang, Q.; Peng, X.; Turng, L.S. Highly Efficient Removal of Methylene Blue Dye from an Aqueous Solution Using Cellulose Acetate Nanofibrous Membranes Modified by Polydopamine. *ACS Omega* **2020**, *5*, 5389–5400. [CrossRef]
70. Eltaweil, A.S.; Abd El-Monaem, E.M.; Omer, A.M.; Khalifa, R.E.; Abd El-Latif, M.M.; El-Subruiti, G.M. Efficient removal of toxic methylene blue (MB) dye from aqueous solution using a metal-organic framework (MOF) MIL-101 (Fe): Isotherms, kinetics, and thermodynamic studies. *Desalin. Water Treat.* **2020**, *189*, 395–407. [CrossRef]
71. Jahangiri, M.; Adl, J.; Shahtaheri, S.J.; Rashidi, A.; Ghorbanali, A.; Kakooe, H.; Forushani, A.R.; Ganjali, M.R. Preparation of a new adsorbent from activated carbon and carbon nanofiber (AC/CNF) for manufacturing organic-vacbpour respirator cartridge. *Iran. J. Environ. Health Sci. Eng.* **2013**, *10*, 15. [CrossRef]
72. Mane, V.S.; Mall, I.D.; Srivastava, V.C. Kinetic and equilibrium isotherm studies for the adsorptive removal of Brilliant Green dye from aqueous solution by rice husk ash. *Environ. Manag.* **2007**, *84*, 390–400. [CrossRef]
73. Hasani, N.; Selimi, T.; Mele, A.; Thaçi, V.; Halili, J.; Berisha, A.; Sadiku, M. Theoretical, Equilibrium, Kinetics and Thermodynamic Investigations of Methylene Blue Adsorption onto Lignite Coal. *Molecules* **2022**, *27*, 1856. [CrossRef]
74. Tuba, B.; Ucun, H.; Baris, H. Removal of methylene blue onto forest wastes: Adsorption isotherms, kinetics and thermodynamic analysis. *Environ. Technol. Innov.* **2021**, *22*, 101501. [CrossRef]
75. Langmuir, I. The Constitution and Fundamental Properties of Solids and Liquids. Part I. Solids. *J. Am. Chem. Soc.* **1916**, *38*, 2221–2295. [CrossRef]
76. Freundlich, H. Über die Adsorption in Lösungen. *Z. Für Phys. Chem.* **1907**, *57*, 385–470. [CrossRef]
77. Temkin, M.I. Kinetics of ammonia synthesis on promoted iron catalysts. *Acta Physiochim. URSS* **1940**, *12*, 327–356.
78. Basso, T.; Beatriz, H.; Freitas, E.; Januário, D.; Bergamasco, R.; Marquetotti, A.; Vieira, S. Green synthesis of copper oxide nanoparticles using *Punica granatum* leaf extract applied to the removal of methylene blue. *Mater. Lett.* **2019**, *257*, 126685. [CrossRef]
79. Thakur, P.; Kumar, V. Kinetics and thermodynamic studies for removal of methylene blue dye by biosynthesize copper oxide nanoparticles and its antibacterial activity. *J. Environ. Heal. Sci. Eng.* **2019**, *17*, 367–376. [CrossRef]
80. Fazal, T.; Razzaq, A.; Javed, F.; Hafeez, A.; Rashid, N.; Amjad, U.S.; Rehman, M.S.U.; Faisal, A.; Rehman, F. Integrating adsorption and photocatalysis: A cost effective strategy for textile wastewater treatment using hybrid biochar-TiO_2 composite. *J. Hazard. Mater.* **2020**, *390*, 121623. [CrossRef] [PubMed]

81. Mansour, A.T.; Alprol, A.E.; Abualnaja, K.M.; El-beltagi, H.S.; Ramadan, K.M.A.; Ashour, M. The Using of Nanoparticles of Microalgae in Remediation of Toxic Dye from Industrial Wastewater: Kinetic and Isotherm Studies. *Materials* **2022**, *15*, 3922. [CrossRef]
82. Xie, S.; Li, W.; Pan, Z.; Chang, B.; Sun, L. Mechanical and physical properties on carbon nanotube. *J. Phys. Chem. Solids* **2000**, *61*, 1153–1158. [CrossRef]
83. Davarnejad, R.; Azizi, A.; Asadi, S.; Mohammadi, M. Green synthesis of copper nanoparticles using *Centaurea cyanus* plant extract: A cationic dye adsorption application. *Iran. J. Chem. Chem. Eng.* **2022**, *40*, 1–14. [CrossRef]
84. Li, L.H.; Xiao, J.; Liu, P.; Yang, G.W. Super adsorption capability from amorphousization of metal oxide nanoparticles for dye removal. *Sci. Rep.* **2015**, *5*, 9028. [CrossRef]
85. Zhao, M.; Tang, Z.; Liu, P. Removal of methylene blue from aqueous solution with silica nano-sheets derived from vermiculite. *J. Hazard. Mater.* **2008**, *158*, 43–51. [CrossRef]
86. Kumar, K.V.; Ramamurthi, V.; Sivanesan, S. Modeling the mechanism involved during the sorption of methylene blue onto fly ash. *J. Colloid Interface Sci.* **2005**, *284*, 14–21. [CrossRef]
87. Yao, Y.; Xu, F.; Chen, M.; Xu, Z.; Zhu, Z. Adsorption behavior of methylene blue on carbon nanotubes. *Bioresour. Technol.* **2010**, *101*, 3040–3046. [CrossRef]
88. Ragadhita, R.; Nandiyanto, A.B.D. How to calculate adsorption isotherms of particles using two-parameter monolayer adsorption models and equations. *Indones. J. Sci. Technol.* **2021**, *6*, 205–234. [CrossRef]
89. Abbasi Pirouz, A.; Selamat, J.; Sukor, R.; Noorahya Jambari, N. Effective Detoxification of Aflatoxin B1 and Ochratoxin A Using Magnetic Graphene Oxide Nanocomposite: Isotherm and Kinetic Study. *Coatings* **2021**, *11*, 1346. [CrossRef]
90. Dashamiri, S.; Ghaedi, M.; Dashtian, K.; Rahimi, M.R.; Goudarzi, A.; Jannesar, R. Ultrasonic enhancement of the simultaneous removal of quaternary toxic organic dyes by CuO nanoparticles loaded on activated carbon: Central composite design, kinetic and isotherm study. *Ultrason. Sonochem.* **2016**, *31*, 546–557. [CrossRef]